



On the stability and accuracy of high stiffness rendering in non-backdrivable actuators through series elasticity



Fabrizio Sergi ^{*}, Marcia K. O'Malley

Mechatronics and Haptic Interfaces Laboratory, Department of Mechanical Engineering, Rice University, Houston, TX 77005, United States

ARTICLE INFO

Article history:

Received 17 February 2014

Accepted 30 January 2015

Available online 20 February 2015

Keywords:

Compliant actuators

Haptics

Coupled stability

Force control

ABSTRACT

This paper addresses the problem of accuracy and coupled stability of stiffness-controlled series elastic actuators, where the motor is modeled as a non-backdrivable velocity source, and the desired value of virtual stiffness is above the physical stiffness of the compliant element. We first demonstrate that, in the mentioned conditions, no linear outer-loop force control action can be applied on the velocity-sourced motor to passify the system. Relaxing the constraint of passivity, we exhaustively search the control design space defined by parametric force and stiffness controllers, expressed in a general lead-lag form, and define a lead-type stiffness compensator that results in acceptable conditions for both coupled stability and accuracy. We also address the effect of a non-ideality in the velocity control loop, such as limited-bandwidth velocity control, and derive relationships between the value of the inner velocity loop time constant and parameters of the stiffness compensator that provide the best performance in terms of both stability and accuracy of haptic display.

We show that the parameters of a simple outer-loop stiffness compensator can be optimized to result in a stable and accurate display of virtual environments with stiffness values in a large range, that also comprises values of virtual stiffness *higher* than the physical stiffness of the compliant element. A requirement for coupled stability is that the actuator is designed such that the minimum value of inertia connected to the compliant actuator load is higher than a control-defined threshold. Finally, we extensively analyze how the minimum value of interaction mass for coupled stability can be minimized through modulation of the stiffness compensator zeros and poles, considering realistic limitations in the velocity control bandwidth of non-backdrivable motors. Our analysis, validated through both numerical simulations and experiments, opens the possibility for alternative approaches to the design of compliant actuators, whereby rendering of high stiffness is possible if the load mass is always higher than a determined threshold.

© 2015 Elsevier Ltd. All rights reserved.

1. Background

The possibility of safe physical interaction and successful cooperation with humans is among the most promising and exciting frontiers of robotics. Several new scenarios such as rehabilitation robotics [1–3], human augmentation robotics [4], surgical robotics [5,6] and haptics have rapidly transitioned from science-fiction, to research laboratories to flourishing industries. In all those scenarios, a common underlying feature is the need of regulating the physical interaction between a human and a robot.

In order to achieve this goal, interaction control approaches, as described in the impedance control framework [7], have extensively been implemented, and their effectiveness demonstrated in

several applications requiring physical interaction with humans. In the case of simple impedance control [7,8], the controller is defined in impedance causality, and the mechanism is modeled as a pure source of effort variables. Successful implementation of this type of impedance controller has been demonstrated mostly in the case of robots with negligible intrinsic dynamical properties or whose motion is approximated by quasi-static movements [1,9,3].

The problem of accurately regulating interaction becomes more difficult in the case of manipulators with complex dynamics, with high inertia, and/or with highly non-transparent actuation systems [10]. When robots are intended for applications requiring substantial assistance to humans during load-intensive tasks, manipulators are indeed not pure effort sources, due to the lack of actuation systems that allow achievement of high force density without substantial increase of task-space dynamic loading. In this

^{*} Corresponding author. Tel.: +1 713 348 2300.

E-mail address: fabs@rice.edu (F. Sergi).

case, model-based dynamic compensation schemes for impedance control can be adopted [11], but often do not fully guarantee accurate interaction control. In general, effectiveness of model-based schemes is limited by neglect of higher order or nonlinear dynamical effects, and by issues related to sensorization and practical limitations in the capabilities of full state feedback, required for compensation of inertial loads.

Force feedback, an approach pursued since the late 1970s [12], can enable the accurate regulation of interaction also in non-transparent manipulators. In such architectures, an explicit measurement of the force of interaction between the manipulator and the environment is used to generate a command signal, that ultimately regulates interaction with the environment. Since then, several forms have been proposed for the force controller, such as proportional control, pure integral control, proportional-integral (PI) control [11], and controllers with inner motion-control loops ([13,14] for compliant joints, and [15] for rigid actuators).

1.1. Passivity for force-feedback systems

Real-world implementations of interaction control through force-feedback do not succeed in achieving arbitrary impedance values. In practice, when a controller attempts to emulate dynamics that differ significantly from those of the hardware, the risk of instability increases [16]. The stability limits in force-feedback controlled systems have been approached through the concept of passivity, a concept adapted from classical theory of electrical networks [16]. It has been proved that when two stable systems with passive impedance port function are coupled together, the coupled system, that results from the connection of the two systems, is stable. Instead, if a robot is stable but non-passive, there will be at least a passive environment that, during interaction, will destabilize the controlled system [16,17]. Proving passivity of a controlled system ensures stability for a wide range of interaction environments that include human dynamics, that are generally modeled as a passive, non linear, first- or second- order system. Also, passivity can be proved for a simplified model, that includes only the controlled system, and do not require detailed knowledge of the environment. Despite the introduced simplicity, this approach allows derivation of strong conclusions on the stability properties of the robot, when coupled to an extremely large and useful set of environments.

Requiring passivity has also drawbacks. Colgate showed that if endpoint force feedback is used to compensate for also the distal mass, the system becomes non-passive [17]. This limitation results from the often unavoidable presence of dynamics between the force sensor and the actuator, that can severely limit the performance of force and impedance controllers. Achievement of global passivity properties for a controller (i.e. passivity for all frequencies) is considered an important requirement for human-interacting robots; yet, at the same time, it is also acknowledged to be quite conservative [18]. It is indeed recognized that the frequency-domain passivity requirement often poses excessive limitations on performance. Examples of approaches violating the frequency-domain passivity requirement without limitations of coupled stability are time-domain passivity controllers [18], also implemented in teleoperation systems [19], and force-feedback controllers for wrist robots [20].

1.2. Inclusion of physical compliance for interaction control

An alternative approach to improving the reflected dynamics of manipulators requires considerable changes to actuators design, as done in Series Elastic Actuators (SEA) [21,22], where a compliant element is introduced in series between the actuator and the load and its deflection measured. This measurement enables estimation

of the interaction forces exchanged between the actuator and the environment, and ultimately of the interaction forces between the human and the robot.

SEAs were originally proposed for their mechanical advantages over stiff actuators, such as shock tolerance and increased power capabilities [21,23,24]. In later years, several research groups showed that Series Elastic Actuators can be successfully employed for accurate implementation of interaction control approaches with actuation systems that could not be modeled as low-impedance effort sources [25–27]. From a control perspective, the primary advantage of series elasticity over stiff force feedback is that the compliant force sensor reduces the physical gain of the feedforward path in the force control loop. In this way, the control gain can be proportionally increased to maintain the overall loop gain of the actuator, resulting in the same stability margins with higher control gains [22]. SEAs can then display a lower output impedance than the one of the actuator alone, without imposing the same stringent limits on the maximum reduction of endpoint inertia as is the case for systems with stiff force-feedback. In fact, this scheme allows simultaneous adoption of high-g geared motors and achievement of low apparent load inertia, since motor inertia is decoupled from the load through the series elastic element.

Though the requirement on minimum reflected inertia for coupled stability does not apply to SEAs, it has been demonstrated that, if inner velocity loops are introduced in the control architecture, the SEA is not passive if it attempts to regulate a behavior corresponding to a pure spring with elastic constant higher than that of the physical compliant element [14]. In the following, we will refer to this case as “virtual stiffness control”, in which it is desired to regulate the force of interaction F_i , in a way that it is proportional to the error between the measured position x and a desired position x_{des} through a constant K_{des} , named virtual stiffness, so that $F_i = K_{des}(x_{des} - x)$. Although different passivity conditions are obtained through alternative controllers types, the presence of inner velocity loops is often mandatory. This is certainly the case of non-backdrivable actuators which can be more suitably modeled in admittance causality, such as piezoelectric actuators. Practical examples of such velocity-sourced motors are ultrasonic piezoelectric motors, such as the one commercialized by Shinsei and utilized in MR-compatible robotics applications [28,29]. For this class of actuators, cascaded force–velocity represents the most direct implementation of an interaction controller. Unfortunately, the limit on passivity (achieved only for $K_{des} \leq k_s$) poses a stringent limitation on the maximum stiffness that can be accurately rendered through a compliant actuator that includes a non-backdrivable motor.

This paper investigates the consequences arising from the violation of the passivity requirement, when the actuated system is controlled to render a pure virtual stiffness with elastic constant higher than the physical spring of the SEA. The analysis is conducted for non-backdrivable motors that are modeled as ideal velocity sources, for which it is possible to derive the parameters of a stiffness compensator capable of achieving coupled stability with a wide range of passive environments. The approach is finally validated through both numerical simulations and experiments in a 1-DOF test bench.

2. Modeling and problem definition

The schematic of a SEA is presented in Fig. 1, in which an actuator drives the output mass through a spring-mass-damper system. The compliant actuator regulates the force of interaction with the environment F_L through measurement of x_M and x_L , representing motor and load displacements, respectively. Assuming knowledge

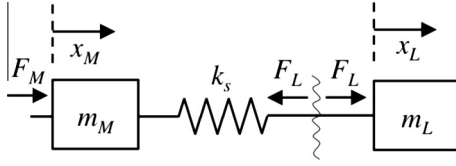


Fig. 1. Mechanical schematic of a Series Elastic Actuator. A motor is connected to the load through a spring, whose deflection is measured, thus allowing measurement of the interaction force F_L .

of the spring elastic constant k_s , F_L is estimated through Hook law: $F_L = k_s(x_L - x_M)$.

The goal is to develop a controller which is able to regulate the apparent impedance $Z_L = \frac{F_L}{\dot{x}_L} = \frac{k_s(x_L - x_M)}{\dot{x}_L}$ of the system at the port of interaction with the environment, (i.e. at coordinate x_L), through only measurement of the two positions x_L and x_M . In particular, we are interested in the possibility of rendering the behavior of a pure spring, with virtual constant K_{des} higher than that of the physical spring, k_s . The environment is defined by the mass m_L in the figure, but it could be any linear passive environment, (i.e. any combination of spring and mass). To this aim, we will investigate whether there are control actions that guarantee passivity of the transfer function Z_L , that would consequently imply stability of the system when coupled to any passive environment.

3. Cascaded force–velocity control

Several control approaches have been proposed for force control of SEAs, including direct feedback force controllers with feedforward compensation [30], nonlinear compensators capable of reducing the effects of friction and variability of interaction dynamics [31] and cascaded linear force-position [32] or force-velocity control [33,13,34]. In the specific case of SEAs designed to improve the interaction control performance of non-backdrivable or high impedance actuators, the latter two controllers are of particular interest, since they effectively allow the conversion of a force control problem into simpler position or velocity control problems, thereby enabling the implementation of interaction controllers for non-transparent motors. The cascaded force and velocity control scheme was demonstrated to be passive [34] for a wide range of desired impedance values. This holds true even in the absence of viscous friction, which is not generally the case of direct force/torque feedback control [35].

Fig. 2 reports a general block diagram of the cascaded force-velocity controller for an SEA in the Laplace domain, C_Z and C_F being the transfer functions of the stiffness and force controller, respectively. The inner velocity loop can be modeled by the superposition of two contributions, one describing velocity control performance, and the other describing the degradation of velocity control due to the interaction with the environment:

$$V_M(s) = H_v(s)V_{des}(s) + D_v(s)F_L(s), \quad (1)$$

where H_v is the velocity control closed loop transfer function, in the absence of torque disturbance, and D_v describes the effect of torque disturbance on velocity control output.

For non-backdrivable motors, within their linear range, the effect of velocity reduction provided by interaction with the environment is negligible. Such simplification is accurate for a class of actuators such as piezoelectric actuators, which have a very small intrinsic admittance both in their unpowered and in their velocity-controlled modes [36]. In order to model this effect, we will assume perfect disturbance rejection from the velocity controller, and we will assume that the term $D_v(s)F_L(s)$ is negligible compared

to the first term in (1), implying no effect deriving from load torque on the motor velocity control performance.

Under the mentioned assumptions, the velocity-controlled ultrasonic motor has been modeled as an ideal velocity source, as described in the block diagram shown in Fig. 2, assuming that $D_v = 0$. In order to regulate interaction, an outer loop is then closed on the measurement of the load position x_L , which is compared to the desired load position, in order to define a desired force value F_{des} , determined as a stiffness force field converging towards the desired position x_{des} . In interaction control, it is often desired to regulate mechanical interaction between subjects and the robot by specifying different values of virtual stiffness K_{des} , thereby regulating the level of mechanical assistance towards the equilibrium position provided by the robot. In the following, we will analyze which are the limits of virtual stiffness values that can be rendered in a stable manner, and design control actions to improve stability and accuracy of stiffness control.

3.1. Limitations of pure stiffness control through cascaded force–velocity control

The most straightforward way to implement a stiffness controller through the block diagram shown in Fig. 2 is to impose $C_Z = 1$. Correspondingly, the outer stiffness loop will be commanding elastic desired interaction forces, displaying a force field proportional to the difference between the desired load position and the measured load position, with an arbitrary stiffness constant K_{des} . In this case, using a proportional controller as force compensator (i.e. $C_F = k_{pf}$), the impedance of the controlled system Z_L can be calculated as:

$$Z_L = \frac{k_s s + (K_{des} k_{pf} k_s)}{s^2 + (k_{pf} k_s) s} \quad (2)$$

Analysis of the passivity of the controlled system impedance transfer function allows determining the coupled stability during interaction with passive environments. In order for the controlled system to be passive, the impedance transfer function Z_L needs to be stable and to satisfy the condition $\text{Re}(Z_L(j\omega)) > 0, \forall \omega \in \mathbb{R}$. Through symbolic calculation, assuming $s = j\omega$, we can calculate the real part of the Z_L transfer function, and evaluate conditions for it to be positive, hence concluding on the passivity of the system. We obtain

$$\text{Re}(Z_L(j\omega)) = \frac{k_s k_{pf} (k_s - K_{des})}{\omega^2 + (k_{pf} k_s)^2}, \quad (3)$$

which is clearly positive only for $k_s > K_{des}$, for all values of the force compensator gain. The same result can be derived for a force compensator that includes a proportional-integral controller, as the one proposed for passive interaction control of SEAs [14]. Hence, the system is not passive if it is commanded to render a virtual spring with stiffness higher than that of the physical spring.

4. Coupled stability and performance during display of high-stiffness environments

The analysis of the Bode plot of the impedance transfer function of the controlled system is shown in Fig. 3. It can be seen that when $K_{des} > k_s$, the impedance transfer function approximates a pure spring at low frequencies, and becomes a non-passive transfer function (with phase lower than -90 deg) above a certain frequency value, that can be modulated through action on the force feedback compensator gain.

In order to guarantee stability during rendering of a high-impedance environment, we relax the constraints on the specific form of force and stiffness compensators, and conduct an analysis

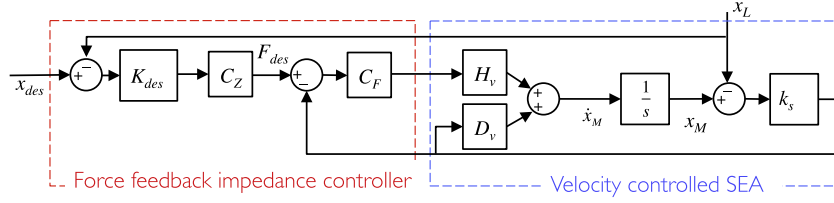


Fig. 2. Block diagram of the controlled system. A non-backdrivable motor is controlled to be a velocity source, and an outer loop is closed on the measured force of interaction with the environment. A velocity control disturbance transfer function can be defined to describe the effect of interaction force on error in velocity control. This function will be neglected, assuming negligible admittance for the velocity controlled motor.

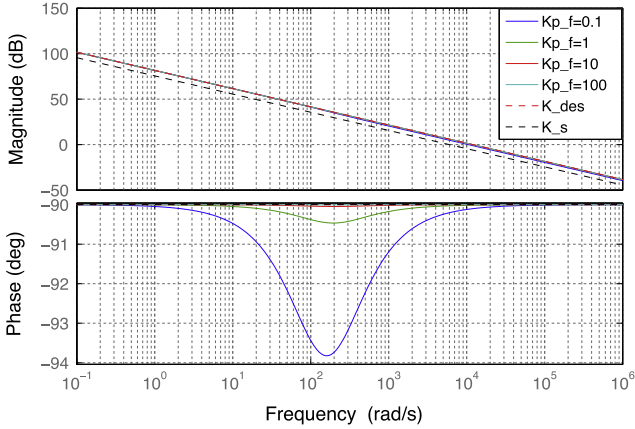


Fig. 3. Bode diagram of the apparent impedance of the system, when controlled through the proportional impedance compensator, $F_{des} = -K_{des}(x_L - x_{des})$, with a proportional force feedback compensator $C_F = k_{pf}$.

in which we will assume them to be generic, causal compensators C_F (for the force compensator), and $K_{des}C_Z$ (for the stiffness compensator), and consider a causal rational polynomial expression for the velocity control transfer function H_v . The virtual impedance Z_L rendered at the load side, is given by:

$$Z_L(s) = \frac{k_s}{s} \frac{s + K_{des}C_F H_v C_Z}{s + k_s C_F H_v} = \frac{k_s}{s} K(s) \quad (4)$$

Analysis of (4) provides significant insight on the behavior of the system. In particular, the first term defines the physical properties of the system reflected to the output: a pure spring with stiffness k_s . In contrast, the second term, labeled as $K(s)$, is a transfer function that describes how the physical stiffness is modulated to be displayed to the output. If $K(s) = 1$, the system displays a stiffness exactly equal to that of the physical spring. Modulations in the amplitude of $K(s)$ allow regulation of different stiffness values. If the phase of $K(s)$ is positive, this will add damping to the system, whereas if the phase of $K(s)$ is negative, this will contribute to further decreasing the phase of the impedance transfer function Z_L below its value of -90 deg dictated by the pure integral action of the spring. In particular, it should be noted that, unlike the case of servo controls, the transfer function of force and impedance compensators do not enter linearly into the open-loop transfer function $Z_L Y_e$ (that determines stability of the system when coupled to the environment with admittance Y_e), nor into the transfer function Z_L (that determines performance of the haptic display). This limitation is, in general, inherent to interaction controllers [10] that operate without a specific model of the environment. This makes design of a controller aimed at regulating interaction with an unknown environment a difficult task that cannot be addressed with traditional methods borrowed from the servo controllers literature.

It is useful to analyze how the conditions for accuracy and passivity translate into requirements for the $K(s)$ transfer function. For

pure stiffness control, it is desired to render a pure spring, with stiffness K_{des} . In this case, the performance condition is:

$$Z_L(\omega) = \frac{K_{des}}{j\omega}, \quad \omega \in \Omega_c, \quad (5)$$

where Ω_c is a range of frequencies of interest, for which it is desired to accurately regulate interaction. The condition for passivity of the haptic display dictates that the apparent stiffness fraction $K(s)$ needs to satisfy the following relation, $\forall \omega$:

$$0 < \arg K(\omega) < \pi \quad (6)$$

We now evaluate how the choice of compensators C_F and C_Z allows fulfillment of coupled stability during interaction with the environment. We will focus on the case $K_{des} > k_s$, which is a challenging condition for which to ensure coupled stability. In fact, it can be intuitively demonstrated that no choice of causal, finite-magnitude compensators C_F and C_Z allows fulfillment of the passivity requirement with the cascaded force-velocity control scheme. In fact, if C_F and C_Z have finite magnitude response at all frequencies, $\lim_{s \rightarrow \infty} K(s) = 1$, which implies that at high frequencies, the apparent stiffness of the system reduces to the physical stiffness of the series elastic element. However, for the case in which the desired stiffness is higher than the physical stiffness of the spring (i.e. $K_{des} > k_s$), the modulus of the stiffness transfer function $|K|$, within the range of frequencies Ω_c will be such that $|K(\omega_1)| > |K(\omega)|, \forall \omega_1 \in \Omega_c, \omega > \max(\Omega_c)$. Hence, for $K_{des} > k_s$, the imposition of the performance requirement implies that $K(s)$ is required to have a flat, zero-phase region at low frequencies, with amplitude $K_{des}/k_s > 1$, and a second flat, zero-phase region (above the frequency band Ω_c where performance is specified), of unitary amplitude. Due to a fundamental property of Bode plots, the two zero-phase regions (higher amplitude at lower frequencies and lower amplitude at higher frequencies) cannot be simultaneously present in a system, without the phase diagram having at least one point with negative phase. It is thus not possible, with the reported control approach, to render accurate, zero damping, haptic display, with stiffness $K_{des} > k_s$, respecting the passivity requirement. The mentioned limitation has profound consequences: from the analysis of the closed-loop transfer function $Z_L Y_e$, it can be demonstrated that, subject to proportional force control $C_F = k_{pf}$ and to the implementation of pure stiffness control ($C_Z = 1$), the system is unstable when coupled to any environment consisting of a mass $m_e > 0$ (i.e. the worst possible coupled stability result).

4.1. Role of force compensator on coupled stability

Not every choice of force and stiffness compensators C_F and C_Z implies coupled instability with every value of environment mass. We will demonstrate this through two separate analyses that consider different choices of compensators C_F and C_Z . Let us first assume the following structure for the force compensator:

$$C_F = k_{pf} \frac{s + Z_F}{s + p_F} \quad (7)$$

Through this expression, the force compensator is expressed by a transfer function with one zero and one pole that can take the form of a lead compensator (for $z_F < p_F$), a lag compensator (for $z_F > p_F$), a proportional controller $p_F = z_F$, a proportional-integral action (for $p_F \rightarrow 0$) and a causal derivative action (for $z_F \rightarrow 0$). For this controller, the impedance transfer function Z_L^f obtained under the effect of the force compensator is:

$$Z_L^f(s) = \frac{k_s s^2 + (k_s p_f + K_{des} k_{p,f} k_s) s + K_{des} k_{p,f} k_s z_f}{s^3 + (p_f + k_{p,f} k_s) s^2 + (k_{p,f} k_s z_f) s}, \quad (8)$$

which, in agreement with the general demonstration presented in Section 4, is not passive for any choice of the control parameters $k_{p,f}$, p_f and z_f , when $K_{des} > k_s$. It is interesting to observe the coupled instability of the system, when it is interacting with its most destabilizing environment. It can be verified that for this stiffness controlled system, the most destabilizing environment is a pure mass, i.e. the admittance $Y_e = \frac{1}{m_e s}$. In this condition, the closed-loop system is unstable for every value of interacting load mass $m_e > 0$, for every value of the controller parameters. In fact, through calculation of the characteristic polynomial $CLP = 1 + Z_L^f Y_e$ and application of the Routh-Hurwitz stability criterion to the coefficients of its numerator, it is possible to simplify the resulting system of inequalities to the simple expression: $K_{des} \leq k_s$.

This demonstrates that coupled stability can be obtained only for values of desired stiffness less than or equal to the stiffness of the physical spring, regardless of the specific choice of the force feedback compensator (i.e. a lead or lag compensator, PI controller or compensator with a derivative action), for every value of interacting mass.

4.2. Coupled stability through stiffness compensator

The simplest method to guarantee stability of the system is through an explicit damping action by the controller, that can be expressed in the form of a velocity-dependent action of the stiffness compensator C_z . This can be obtained, for example, by employing proportional force feedback, and considering the following form for the stiffness controller: $C_z = 1 + \frac{B_{des}}{K_{des}} s$. In this case, the resulting system can be made passive for certain values of desired stiffness K_{des} . In fact, the impedance transfer function Z_L^b , under the action of the damping action is:

$$Z_L^b = \frac{(k_s + B_{des} k_{p,f} k_s) s + K_{des} k_{p,f} k_s}{s^2 + k_{p,f} k_s}, \quad (9)$$

which is passive also when $K_{des} > k_s$, if the controller is introducing an amount of damping higher than the threshold B^* , defined as

$$B^* = \frac{K_{des} - k_s}{k_{p,f} k_s}. \quad (10)$$

Some practical limitations arise from the adoption of this controller. First, if no direct measurement of velocity is assumed, the anti-causal damping action cannot be practically implemented in real systems. Practically, the damping term will be implemented as a causal derivative action, which behaves as a pure differentiator¹ at low frequencies, and reduces to a proportional gain at higher frequencies, as provided by the causal differentiator transfer function $G = \frac{Ns}{s+N}$. Introducing the non-ideal differentiator transfer function in the impedance compensator, we then lose again the possibility of proving passivity for the impedance-controlled system

¹ We are neglecting the effect of the required low-pass filtering and delay that is needed to differentiate digital position signals deriving from encoders, that are affected by quantization.

for every $K_{des} > k_s$. Indeed, the effect of a non-ideal compensation term is significant. Because of the introduction of the damping B_{des} , it can be shown that for every finite value of N , coupled instability will occur for every value of environment mass $m_e > 0$, i.e. the worst-possible coupled stability result. This issue can be mitigated by introducing damping in the system in excess, compared to what is required in theory in (10). However, this solution would reduce the accuracy of haptic display also at low frequencies, where in theory no damping action would really be needed for coupled stability. In order to address the limitations of this pure damping action, we will then investigate the effect of the introduction of lead and lag in the stiffness compensator, by defining it in the form²:

$$C_z = \frac{p}{z} \frac{s+z}{s+p} \quad (11)$$

In this case, the resulting impedance transfer function, under the effect of the stiffness compensator, Z_L^k is:

$$Z_L^k(s) = \frac{k_s z s^2 + (k_s p z + K_{des} k_{p,f} k_s p) s + K_{des} k_{p,f} k_s p z}{z s^3 + (p z + k_{p,f} k_s z) s^2 + (k_{p,f} k_s p z) s} \quad (12)$$

Again, the introduction of an amplitude-bounded causal compensator C_z , acting on the error between measured and desired load position, results in an impedance transfer function that is passive only if $K_{des} \leq k_s$. However, an analysis of coupled stability of this controller provides results that allow for margins in controller design. In fact, through evaluation of the closed loop polynomial during interaction with the most destabilizing environment (again, a pure mass), and application of the Routh-Hurwitz stability criterion, it can be seen that coupled stability can be obtained for a wide range of interacting mass values, that can be modified by a proper choice of controller gains. Reduction of the Routh-Hurwitz determinants provides the following conditions for coupled stability ($m_e > 0$):

$$\begin{aligned} (1) \quad m_e < m^* \text{ AND } p < \frac{k_s z}{K_{des}} \text{ AND } \left[k_{p,f} \neq \frac{K_{des} z - k_s z}{K_{des} k_s} \right] \\ (2) \quad m_e > m^* \text{ AND } p > \frac{K_{des} k_{p,f} k_s z}{K_{des} k_{p,f} k_s - K_{des} z + k_s z} \end{aligned} \quad (13)$$

$$\text{with } m^* = \frac{k_s (K_{des} k_{p,f} + z) (K_{des} p - k_s z)}{z (k_{p,f} k_s + p) [p z k_s + K_{des} (k_{p,f} k_s (p - z) - p z)]}$$

showing that coupled stability can be obtained as a function of a threshold load mass value m^* . Though this controller cannot be proved stable with arbitrary values of environment mass m_e , it allows modulation of the value of m^* to ensure that the value of admissible environment mass m_e is always within the stability range defined by (13). In particular, the value of m^* can be reduced to guarantee that the second inequality shown in (13) is respected in all operating conditions. Through this control design method, it is possible to guarantee that the system is stable for values of interacting mass higher than a certain threshold.

This approach can be surprisingly useful, since in most SEA designs, the minimum value of interacting mass m_e is never equal to zero due to inherent design constraints (e.g. a linear SEA will have a load plate that will be used to connect to a load; a rotary SEA will be necessarily connected to some output link, whose inertia adds to the load inertia). Moreover, for applications that involve wearable human-interacting robots, such as rehabilitation or human augmentation, the minimum value of mass connected to the load is often significant. For example, the mass might consist of the inertia of the hand for a wrist exoskeleton, or of the inertia of the lower leg for a knee exoskeleton. Using a constant gain

² The symbolic form of the compensator C_z is similar to the one chosen for C_F , but an amplitude normalization factor $\frac{p}{z}$ has been introduced, so as to guarantee that the stiffness displayed at low frequencies matches the desired stiffness K_{des} .

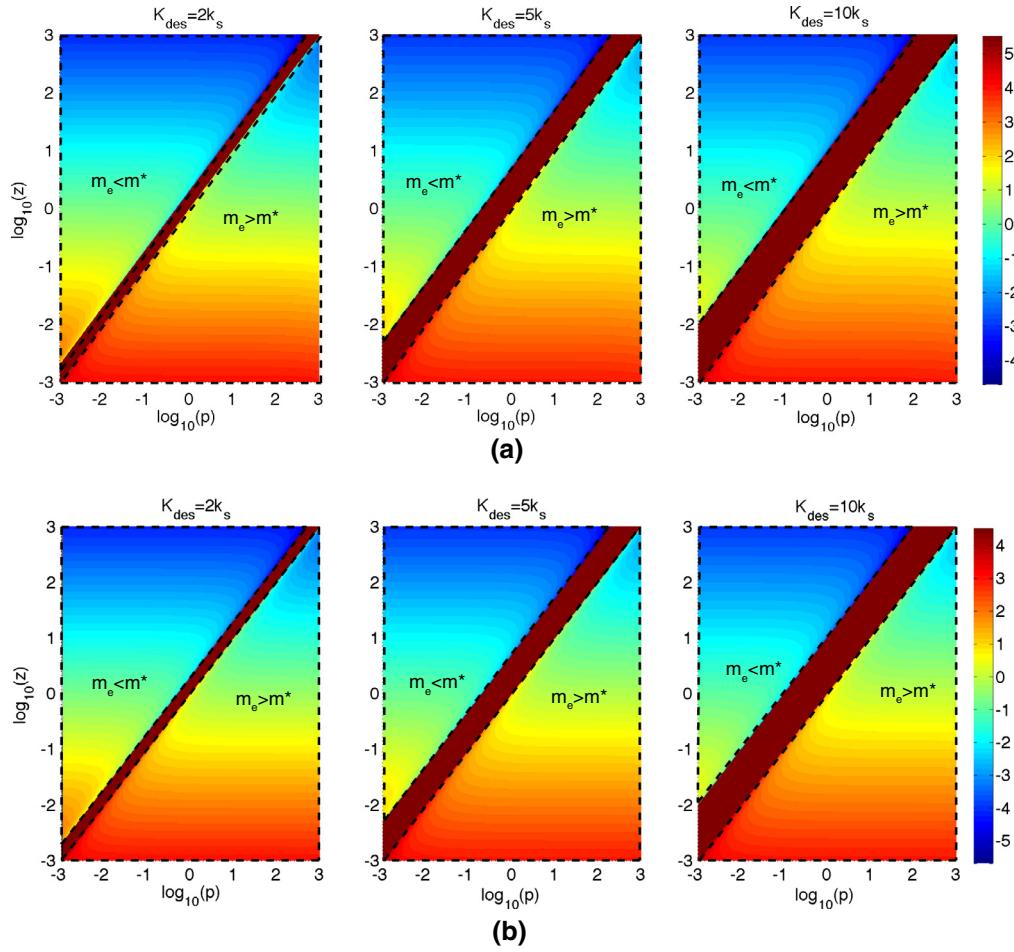


Fig. 4. Logarithmic color maps showing values of threshold environment mass m^* , for coupled stability during stiffness control at different values of K_{des} (columns), for different values of force compensator gains, $k_{pf} = 1$ (a), and $k_{pf} = 10$ (b). Use of lag compensators ($p < z$ – upper-left triangular section of the $p - z$ plane) results in coupled stability for values of interacting mass $m_e < m^*$, while lead compensators ($p > z$ – lower-right triangular section of the $p - z$ plane), result in coupled stability for values of interacting mass $m_e > m^*$. The region where coupled stability is not guaranteed for any value of interacting mass is separated by the dashed line-contoured regions and is reported in dark red. (For interpretation of the references to color in this figure legend, the reader is referred to the web version of this article.)

controller, the system can be made stable with masses whose value can be seen in Fig. 4, parameterized in terms of force feedback gain and desired stiffness value. It can be seen that this control approach allows achievement of coupled stability with a limited set of environments, that can be regulated through control parameters, in a way that the range of admissible values for coupled stability is well contained in the range of interacting environments that can be considered in a given application.

We now investigate which values of minimum and maximum interacting mass m^* that guarantee coupled stability can be obtained with feasible combinations of control parameters. In particular, we conduct this analysis by assuming a fixed value for the force compensator control gain, and investigate the dependency of m^* on the characteristics of the impedance compensator gain, for different values of desired stiffness.

The results of this analysis are shown in Fig. 4, where the regions of compensator values resulting in minimum and maximum values of interacting mass that guarantee coupled stability are contoured by dashed lines. In particular, it can be seen that pure stiffness control $p = z$ would result in coupled instability for every value of interacting mass (dark red region interposed between the two colormap regions where stability is possible for some values of mass).

From the coupled stability standpoint, it would seem that the best choice of C_z could either be that of a lead-compensator, with

one pole and one zero in the high frequency range, or that of a lag compensator, with low-frequency pole and zero. In fact, in the first case ($z < p$), coupled stability is achieved for values of environment mass higher than a threshold, that can be decreased through control gains (i.e. moving p towards higher frequencies and increasing the force-feedback compensator gain k_{pf}). In the second case ($p < z$), coupled stability is achieved for values of environment mass lower than a threshold, which can be again increased through control design (i.e. moving z towards lower frequencies and increasing the force-feedback compensator gain).

Stability is not the only requirement in the design of interaction controllers. Although the stiffness compensator C_z can be designed to have unitary magnitude and zero phase at low frequencies (resulting in an accurate, pure-stiffness interaction behavior at those frequencies), controller parameters can influence the upper limit of this frequency region. To this aim, we define a measure of interaction controller accuracy, as described in [10], and include this measurement within an optimization framework. The framework would optimize the combination of control parameters so as to maximize both performance and stability, that for this specific controller could be defined by the range of masses that result in a stable interaction.

Under the “ideal non-backdriveability, ideal velocity control” hypothesis stated so far, the system has been simplified to the point that it lends itself to an intuitive, straightforward and

informative performance analysis. In fact, from the analysis of the $K(s)$ transfer function, it can be seen that the effect of the impedance compensator is to introduce a phase lead or lag starting at the frequency where the lowest frequency pole or zero of the impedance compensator is located. This can be seen also from the analysis of the impedance transfer function, parameterized as a function of the specific value of compensator gains (that change from a lead compensator to a lag compensator). The analysis can be conducted by keeping the pole location constant, and observing the effect on the resulting impedance transfer function, as a function of the zero location, as reported in Fig. 5. It can be seen that accurate impedance rendering is obtained for $\omega \in (-\infty, \min(p, z)]$, i.e. up to a frequency that depends on the minimum value zero or pole introduced in the compensator. A very simple performance measure can be introduced for this system, as given by the two-dimensional function acc , defined as:

$$\text{acc} = \min(p, z), \quad (14)$$

with its colormap reported in Fig. 6.

From an intersection analysis between the two plots, it is now clear that an acceptable compromise between stability and performance is provided only by a control action of a lead-compensator type (i.e. $p > z$). In fact, this controller allows achievement of accurate interaction up to a frequency $\omega_c = z$, and guarantees coupled stability for interaction masses higher than a certain threshold, that can be reduced through control action to values that are largely lower than the realistic values associated with a given application.

In these conditions, it can be verified by inspection of Eq. (13) that the value of minimum mass required for a stable interaction is linear with the value of virtual stiffness. This means that, once control gains have been tuned, the higher the value of desired stiffness K_{des} , the higher the minimum load mass in order to achieve coupled stability.

4.3. Effect of a non ideal inner velocity loop

We now address the effect of model non-idealities, introducing a high-frequency attenuation in velocity control performance, modeling the velocity control transfer function H_v as a low-pass filter $\frac{1}{s\tau+1}$. We describe the effect of τ on both the accuracy and performance of interaction control. First, we analyze the effect of the inner velocity loop transfer function on the selection of the optimal

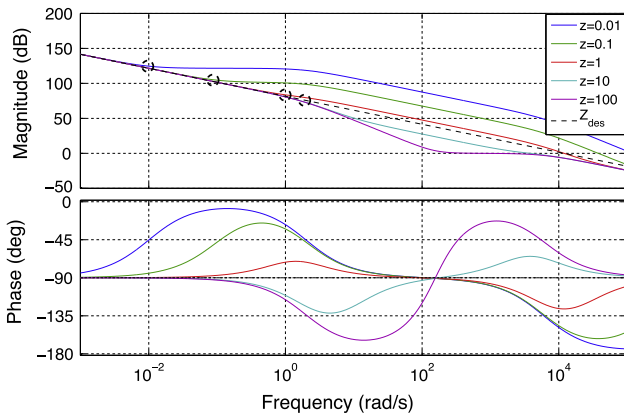


Fig. 5. Resulting impedance transfer function Z_L^k , when $p = 1$ and for different values of z , for a unitary force feedback compensator gain and a desired stiffness $K_{des} = 2k_s$. Circled points are those in which the magnitude of the modulated stiffness transfer function $K(s)$ is attenuated by 3 dB. The frequencies in which this situation occurs are in correspondence with the minimum pole or zero of the impedance compensator.

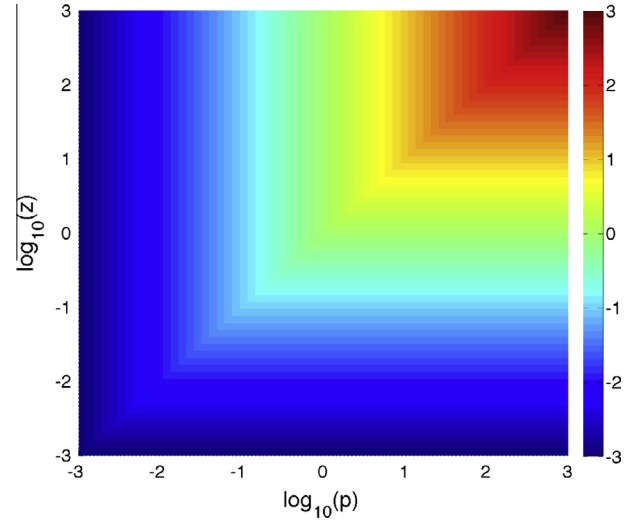


Fig. 6. Measure of accuracy for the interaction controller implemented through the impedance compensator C_z , determined as $\max(p, z)$, in a logarithmic scale. The plotted function represents a quarter of a square pyramid (the lower-left quarter of the pyramid, from the top view shown in the colormap), cut through two orthogonal planes that contain the pyramid axis and one of the axes defined by the basis edge, respectively. The pyramid vertex, i.e. the point $p = p_{MAX}, z = p$, corresponds to the point with highest accuracy.

controller gains that maximize stability and evaluate the effect on the haptic display accuracy. For every set of controller gain values, the minimum value of interacting mass for coupled stability is computed through a root locus analysis, analyzing the interaction with the most destabilizing environment (a pure mass). This can be done by calculating the minimum value of m_e that results in the admittance environment transfer function $Y_e = \frac{1}{m_e s}$ such that the polynomial CLP , that describes the stability of the coupled system, with

$$CLP = 1 + Z_L Y_e \quad (15)$$

has roots in left half complex plane. Also, for every set of controller gain values, a measure of impedance control accuracy is introduced as in [10], as the reciprocal of the cost function, calculated in a logarithmically-spaced set of frequencies of interest $\Omega = \{\omega_1, \omega_2, \dots, \omega_n\}$, $\omega_1 = 10^{-3}$, $\omega_n = 10^3$:

$$C(\omega) = \sum_{i=1}^n |\log |Z_L(j\omega_i)| - \log |Z_{des}(j\omega_i)||, \quad (16)$$

that compares the amplitude of the resulting impedance transfer function Z_L to the desired impedance Z_{des} . The analysis is reported in Fig. 7 for specific values of K_{des} and τ , varying controller gains. The analysis shows that the region of controller gains that maximizes accuracy is, in agreement with the results obtained in the ideal velocity control case, the upper-right corner of the $p - z$ plane, i.e. the region that maximizes p and z , with $p > z$. The introduction of the non-ideal velocity controller slightly modifies the optimality conditions for coupled stability. In fact, minimization of the environment mass for coupled stability is obtained when the compensator zeros/poles are in a lower frequency range. The specific value of the upper limit of this frequency range will depend on the value of the velocity loop transfer function time constant.

To further investigate the issue of optimal zero-pole location in the impedance compensator C_z , we addressed both stability and accuracy, and evaluated how such properties vary as a function of inner velocity loop time constant τ . Once the controller parameters p_{opt}^τ and z_{opt}^τ that yield the minimum value of interacting mass for coupled stability are determined for every value of τ ,

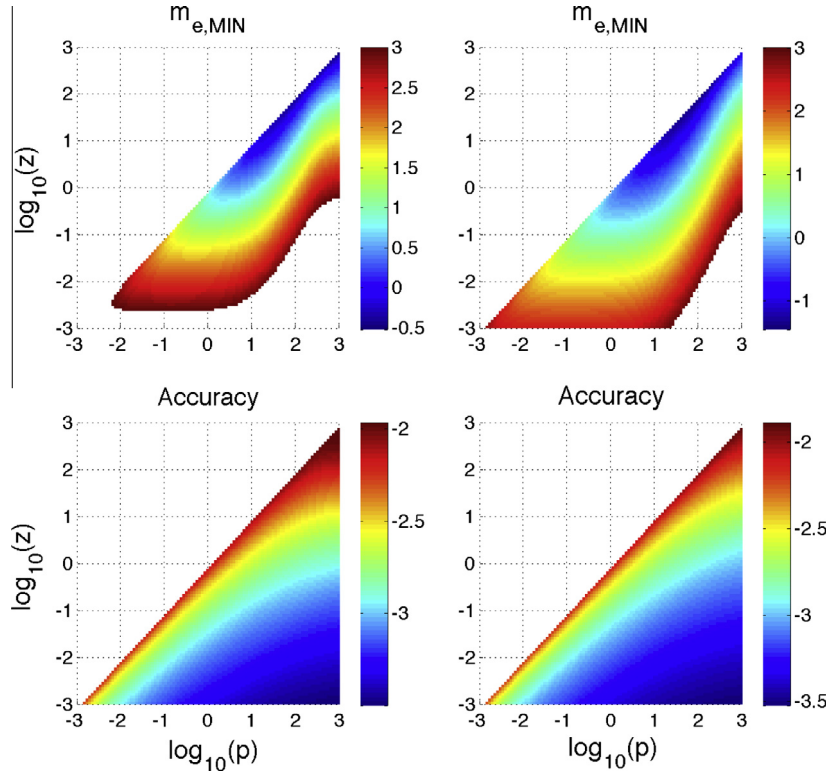


Fig. 7. Effect of stiffness compensator parameters on the minimum value of interacting mass for coupled stability ($m_{e,MIN}$, shown in the top plots) and on the accuracy of the impedance transfer function, defined as $1/C$ – lower plots, for frequencies logarithmically spaced between 10^{-3} rad/s and 10^3 rad/s. An inner velocity loop modeled as a first-order low-pass filter with time constant $\tau = 0.01$ is considered in this analysis, and the value of the force-feedback compensator gain is set to 1 (left) and 10 (right).

the accuracy measure $1/C_{opt}^{\tau}$ of the impedance-controlled system is calculated, and reported (see Fig. 8; labeled as Opt_{τ}). Similar analysis was conducted for the ideal compensator gains obtained for the ideal velocity loop case (labeled as Opt), and for the cases in which the minimum damping B^* , as expressed in Eq. (10), is introduced

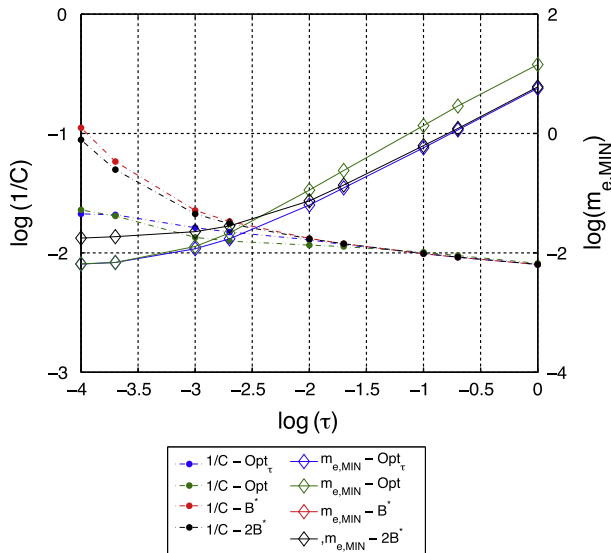


Fig. 8. Effect of different inner velocity loop time constant τ on the accuracy and stability of the impedance controlled compliant actuator. Circle-marked dashed lines represent the performance measure in the left logarithmic scale, while diamond-marked continuous lines represent the stability measure, in the right logarithmic scale.

in the compensator (labeled as B^*), or increased damping equal to $2B^*$ was introduced, labeled as $2B^*$. The analysis is graphically reported in Fig. 8, and enables description of the achievable trade-off between stability and accuracy of high-stiffness impedance control in compliant robots with non-backdrivable actuators, controlled as velocity sources, as a function of the responsiveness of the inner velocity loop.

First, it can be seen that the accuracy and coupled stability requirements are both negatively influenced by slower inner velocity loops. For all considered controllers, a faster inner velocity loop is able to simultaneously provide increased accuracy within the considered frequency range, and lower values of minimum interacting mass for coupled stability (increased stability performance).

A full quantitative comparison between the designed compensator and the system controlled through a pure damping action where the minimum damping B^* is injected in the system is not possible, due to the fact that such a controller results in an unstable system, for all values of interacting mass $m_e > 0$ (due to consideration of frequency-bounded controller derivative action). For this reason, it is not possible to define a measure of stability of this controller.

From a comparison between the results achievable with the two different controllers (i.e. Opt vs. Opt_{τ}), it can be seen that the solution found through separate optimization for different values of τ (Opt_{τ}) provides the best coupled stability results for every value of τ , compared to the controller designed for the ideal velocity loop case (Opt). The amount of reduction in values of minimum mass that provides coupled stability (Δm_e) allowed by the Opt_{τ} controller is very small at low values of τ , ($\frac{\Delta m_e}{m_e} \leq 5\%$, $\tau \leq 0.01$), and becomes more significant while τ increases, settling to $\Delta m_e = m_e$, for the case in which $\tau = 1$.

It can be seen that at low values of velocity control time constant ($\tau < 0.01$), coupled stability can be achieved with very low values of interacting mass, at the expense of haptic display accuracy (the minimum value of interaction mass is reduced in the Opt and Opt_r controllers to less than half of what is allowed with the 2B* controller, but accuracy is reduced by a similar amount). This results from the fact that the range in which control parameters p and z are sought is $[10^{-3} \ 10^3]$ rad/s, representing realistic hardware limitations in real-time control applications. In general, it is shown that the performance obtained through the controller determined for the ideal velocity loop case (Opt) loses its optimality when the region in the frequency domain in which poles and zeros of the outer loop compensator are sought ($[10^{-3} \ 10^3]$ rad/s) overlaps with the region at which the velocity control performance degrades.

5. Model validation

The feasibility of the developed controller is validated through numerical non-linear modeling and simulations, as well as through experiments in a compliant actuator (MR-SEA II) that includes a non-backdrivable traveling-wave ultrasonic motor, a cable transmission and two pre-loaded extension springs.

5.1. System description and modeling

The 1 DOF actuator prototype (MR-SEA II) was developed for an MR-compatible haptics application [36] and is shown in Fig. 9. MR-SEA II comprises a rotary ultrasonic piezoceramic motor (5 W Shinsei ESR60-E3N), a threaded pulley on the motor shaft, a cable transmission, pre-extended phosphor bronze extension springs, a custom-designed Delrin carriage and a linear ceramic balls bearing, supporting the carriage. As shown in the companion design paper [36], the motor is non-backdrivable and when controlled through its own factory-tuned velocity controller can be modeled as a low admittance velocity source, and compensated to regulate velocity linearly (i.e. without amplitude dependence, except for its low velocity region) within its operating frequency and amplitude range (see Table 1). A numerical model is implemented in Simulink (the Mathworks Inc.), and run with an ODE 45 solver at a fixed step of 1 ms, to validate the theoretical analysis assessing the effects of model non-linearities on the closed-loop stability of the system. In the model, the actuator is controlled to display a stiffness K_{des} through the action of the impedance

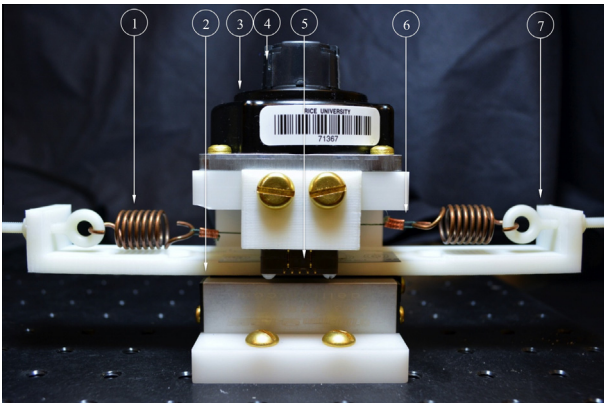


Fig. 9. MR-SEA II. (1) phosphor bronze extension spring, (2) ceramic linear ball bearings, (3) piezoceramic motor, (4) rotary optical encoder, used to measure x_M , (5) linear encoder, used to measure x_L , (6) cable transmission, (7) slider, with plastic eyebolts.

Table 1
MR-SEA performance.

| Property | Value |
|----------------------------------|------------------------|
| Maximum continuous force | 20 N |
| Spring stiffness | 3.8 N/mm |
| Maximum velocity | 0.1 m/s |
| Velocity control frequency range | 0–10 Hz |
| Motor encoder quantization | $1.3 \cdot 10^{-2}$ mm |
| Load encoder quantization | $1 \cdot 10^{-2}$ mm |
| Load mass | 100 g |

compensator C_z acting on the cascaded force–velocity controller, with desired position $x_L = 0$. This controller action responds to a load force perturbation, modeled as a step with amplitude of 4 N (20% of the actuator force capabilities). The case of force perturbation when the compliant actuator is interacting with an environmental mass m_e is chosen because it closely matches the task conducted during the experimental characterization, and because we have demonstrated that it corresponds to the most destabilizing environment for the stiffness-controlled actuator.³ To separate the effects of model non-idealities, the red blocks in Fig. 10 are introduced sequentially in the analysis.

5.1.1. Effect of plant non-idealities through numerical simulations

After checking through fixed-step numerical integration that our theoretical analysis accurately predicts the value of interaction mass resulting in coupled stability, for the lead-lag compensator, and that no proportional stiffness controller can obtain coupled stability for any value of environment mass $m_e > 0$, when $K_{des} > k_s$, we introduce plant non linearities in the numerical model. Firstly, we introduce the saturation block that models the amplitude-dependent limit of velocity control. We determine through a linear search procedure the values of controller parameters that result in coupled stability with the lowest-possible environment mass $m_{e,MIN}^{sat}$. We then analyze what is the effect of the inclusion of two other non-idealities, i.e. the H_V transfer function (resulting in a minimum value of interaction mass m_{th}^{freq} for coupled stability) and, finally, of encoders quantization (resulting in the value of interaction mass $m_{e,MIN}^q$ that provides coupled stability). The results of this analysis are reported in Table 2. When the value of environment mass reduces to only the mass of the slider, it is theoretically possible to achieve coupled stability for values of K_{des} up to $1.75k_s$,⁴ for the MR-SEA II load mass. The presence of the plant non-idealities, and predominantly of the amplitude- and frequency limitation in the actuator inner velocity loop, further increases the minimum value of interaction mass for coupled stability. Given the effect of the limitations of the experimental prototype used to validate this model, only the cases of $K_{des} = 1.25k_s$ and $K_{des} = 1.5k_s$ are considered for the experimental validation.

5.1.2. Experimental validation in the MR-SEA

The optimized control action was implemented in the MR-SEA, using values of desired stiffness K_{des} 25% and 50% higher than the physical stiffness of the spring. The p and z gains from Table 2 corresponding to the lowest-possible value of interaction mass for coupled stability, in the worst case, are chosen (i.e. $p = 500$ for

³ The choice of a particular form of perturbation (e.g. load force perturbation, load velocity perturbation, desired load position) does not change the coupled stability properties of linear systems, since the poles of the closed-loop transfer function are independent of the selected form of perturbation.

⁴ Although a higher range of stable stiffness regulation can be achieved by increasing the value of the force feedback control gain $k_{p,f}$, this case is not considered because the prototype is unstable for higher values of $k_{p,f}$, when $K_{des} < k_s$, due to unmodeled higher-order dynamics.

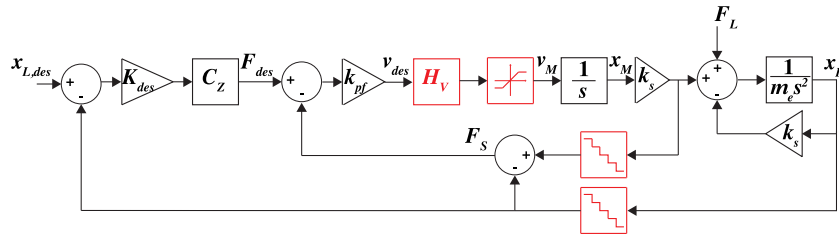


Fig. 10. Block diagram of the numerical model used to validate the theoretical analysis of coupled stability. The blocks describing the plant non-idealities are shown in red, and introduced sequentially in the numerical analysis. (For interpretation of the references to color in this figure legend, the reader is referred to the web version of this article.)

Table 2

Numerical model results – minimum environment mass for coupled stability.

| K_{des} | p (1/s) | z_{best} (1/s) | $m_{e,MIN}$ (kg) | $m_{e,MIN}^{sat}$ (kg) | $m_{e,MIN}^{freq}$ (kg) | $m_{e,MIN}^q$ (kg) |
|-----------|-----------|------------------|------------------|------------------------|-------------------------|--------------------|
| $2k_s$ | 500 | 150 | 0.12 | 0.23 | 0.54 | 0.54 |
| | 250 | 100 | 0.23 | 0.34 | 0.66 | 0.67 |
| | 100 | 50 | 0.58 | 0.60 | 0.93 | 0.94 |
| $1.75k_s$ | 500 | 160 | 0.10 | 0.17 | 0.43 | 0.43 |
| | 250 | 105 | 0.19 | 0.26 | 0.53 | 0.53 |
| | 100 | 52 | 0.48 | 0.48 | 0.75 | 0.76 |
| $1.5k_s$ | 500 | 180 | 0.07 | 0.12 | 0.31 | 0.31 |
| | 250 | 115 | 0.15 | 0.19 | 0.40 | 0.40 |
| | 100 | 55 | 0.37 | 0.37 | 0.57 | 0.58 |
| $1.25k_s$ | 500 | 220 | 0.05 | 0.07 | 0.20 | 0.20 |
| | 250 | 133 | 0.10 | 0.11 | 0.25 | 0.25 |
| | 100 | 62 | 0.26 | 0.26 | 0.40 | 0.40 |

both cases and $z = 220, 180$ for $K_{des} = 1.25k_s$ and $K_{des} = 1.5k_s$, respectively). The stability of the system for these gains is proved in the most destabilizing case, i.e. the application of a constant force to the slider, with instantaneous load removal. In this case, the expected behavior is that of a sustained oscillation of the resulting spring-mass system (note that the stiffness compensator makes no attempt at reducing the load mass), but the energy dissipated through the control action (introduced in order to have the desired stability margins) provides the asymptotic convergence of the slider position – see Fig. 11(a). During high-stiffness display, the MR-SEA was commanded a reference position that was either constant $x_{L,des} = 0$ or oscillating $x_L(t) = A \sin(2\pi f_0 t) - A = 10$ mm, $f_0 = 0.5$ Hz, Fig. 11(b). During the experiment, the subject alternated between the application of a continuous, roughly sinusoidal displacement to the slider and the application of impulsive, impact-like displacement.⁵ The stiffness transfer function $K_v(f)$ was estimated using non-parametric system identification, via the Welch method, using the following relation:

$$\hat{K}_v(f) = \frac{P_{yu}(f)}{P_{uu}(f)}, \quad (17)$$

with $P_{yu}(f)$ the cross-spectral density between the input (u) and output (y) and $P_{uu}(f)$ is the auto-spectral density of the input. To estimate the stiffness transfer function, the load position error $x_{L,des} - x_L$ was selected as input, and the spring force $F_s = k_s(x_L - x_M)$ was selected as output. The estimated transfer function was resampled in a 51-elements, logarithmically spaced frequency vector ([0.01–100] Hz), and normalized dividing by K_{des} , obtaining $\bar{K}_v(f)$. Values of coherence higher than 0.8 were obtained up to approximately 6–7 Hz for both cases of $x_{L,des}$, and a Bode plot of the estimated normalized transfer function is shown in Fig. 11(c).

⁵ This was done in the attempt to excite the system also at frequencies higher than the ones possible through manual perturbation at high stiffness.

In the low-frequency range the system behaves as a pure spring, with elastic constant matching the desired value. The error in virtual stiffness approaches is higher than 3 dB up to a frequency that corresponds to 5–6 Hz, beyond which low coherence values are obtained and the transfer function estimate is no longer reliable. The phase of the estimated transfer function is negative, confirming the non-passivity of the system when $K_{des} > k_s$.

6. Discussion and conclusions

This paper investigates the range of virtual stiffness values that can be stably and accurately displayed by a stiffness-controlled series elastic actuator (SEA), in which the motor is a non backdrivable velocity source. As previously shown in the literature [14], a velocity-sourced SEA can be passively stiffness-controlled to display a virtual stiffness K_{des} , only if $K_{des} \leq k_s$, with k_s being the physical stiffness of the compliant element. In our paper, we start by generalizing this finding, demonstrating that, in the context of linear control theory and with availability of only position information, no outer-loop force control action can be applied on the velocity-sourced system to result in a passive system, when a stiffness value $K_{des} > k_s$ is desired.

We then analyze the effects on coupled stability of a stiffness controller (commanded to impose $K_{des} > k_s$), resulting in a non-passive impedance transfer function. We show that a frequency-limited lead action in the outer-loop stiffness controller results in the best accuracy and coupled stability performance, provided that the system is interacting with a load with inertia higher than a threshold m^* . Through our analysis, we derive the analytical expression that provides the minimum environment mass for stable coupled interaction, when a generic stiffness K_{des} is desired, as a function of the physical stiffness in the actuator and of the controller gains. Our analysis demonstrates that, when $K_{des} > k_s$, the value of minimum environment inertia required for a stable interaction increases with K_{des} with the scaling factor dependent on the choice of the controller gains.

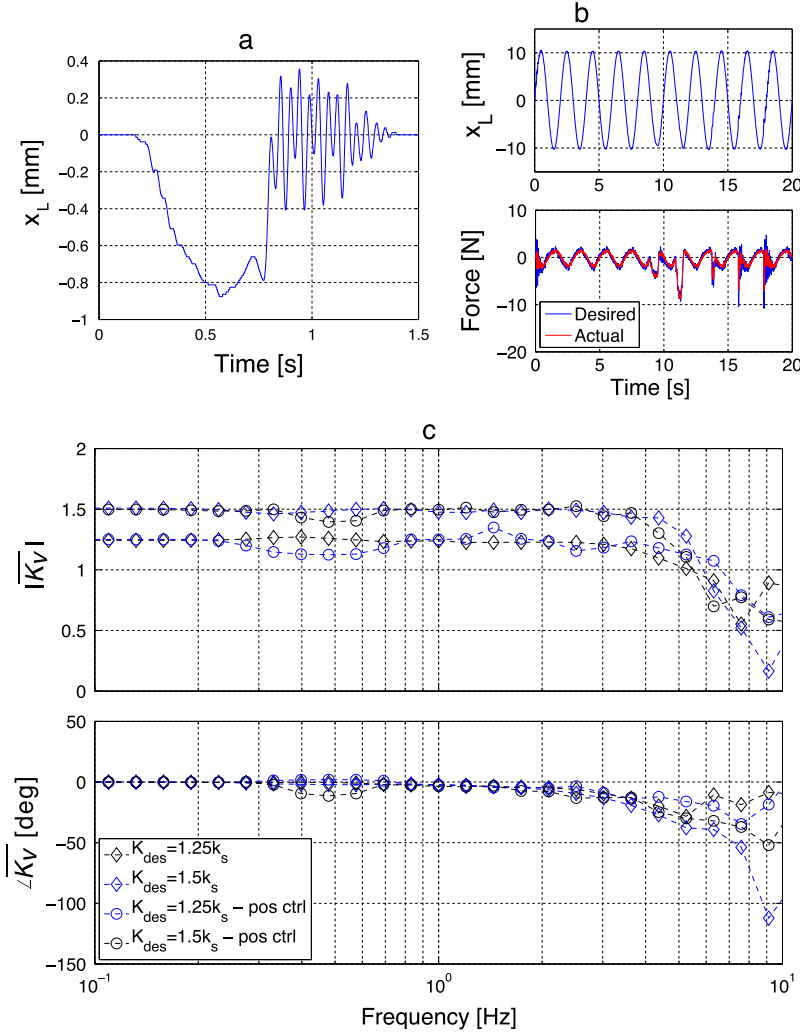


Fig. 11. Experimental validation of the controller in the MR-SEA. (a) Application of an increasing load on the stiffness-controlled MR-SEA ($K_{des} = 1.5k_s$) with instantaneous load removal, resulting in decaying oscillations of the slider. (b) Perturbation of the MR-SEA slider when commanded a sinusoidal position tracking ($K_{des} = 1.5k_s$). After the initial transient, the force error is below 1 N before the subject applies perturbation forces to the slider (after 10 s). The desired force is calculated as $-K_{des}x_L$, and is compared with the measured force, i.e. $k_s(x_L - x_M)$. (c) Bode plot of the estimated normalized stiffness transfer functions, for two values of virtual stiffness and for both position tracking cases.

Using a similar methodology, we address the effect of a non-ideal inner velocity loop on haptic display performance and stability. In particular, we investigate how the minimum value of interaction mass resulting in coupled stability can be minimized through placement of the stiffness compensator zeros and poles, considering realistic limitations in the bandwidth of velocity control, for non-backdrivable motors such as those used in [28] for haptic display of MR-compatible robots. We showed that with knowledge of the frequency limitations of the velocity inner loop (in our case knowledge of the time constant τ of a first-order low pass filter), it is possible to further optimize the stability properties, by significantly reducing the value of minimum mass for a stable interaction, when the pole or zero at higher frequency is one decade below the cut-off frequency of the inner velocity loop.

We finally validate our model through numerical simulations and experiments in the MR-SEA II, a compliant actuator that includes a non-backdrivable piezoceramic motor as a velocity source, demonstrating capabilities for stable rendering of virtual stiffness 50% higher than the physical spring stiffness.

The main result of our analysis is that coupled stability of a stiffness-controlled compliant actuator can be obtained when the actuator is controlled to display a spring with elastic constant

K_{des} , with $K_{des} > k_s$, provided that the minimum value of mass connected to the series elastic element is higher than a threshold, even in absence of friction. This finding is in contrast with an implicit assumption that has guided the development of most compliant actuators for human interaction developed so far. Indeed, in most cases [14,37,38,32,39], the series elastic element has been designed to be substantially stiff, with the idea of then controlling the actuator to display a lower virtual stiffness. The choice of “stiff” springs for SEAs poses challenges on the selection of sensors used to infer interaction force, since they are usually required to have very high resolution, in order to minimize quantization errors in the measurement of interaction forces. Consequently, some of the anticipated benefits deriving from elimination of a traditional force sensor, in terms of reduction in costs and size, can be lost in the attempt of incorporating the sensor(s) required to measure the deflection of the compliant elements.

The results of the presented analysis reveal opportunities for alternative designs of compliant actuators. Given a range of virtual stiffness values that need to be implemented through control, it is not necessary to design the compliant element so that it is stiffer than the stiffest-possible virtual environment for a given application. Instead, the results of this analysis show that the coupled

system will be stable if the system is designed so that it includes a minimum amount of inertia that is connected to the compliant element in all operating conditions. Limitations to this approach can be provided by backlash, or in general of non co-located dynamics, between the series elastic element and the load. In the presence of backlash, the value of load mass instantaneously decreases, potentially to a value that is lower than the threshold for coupled stability, until the control action responds. The energy introduced in the system during impacts, coupled with delays in the position measurement and with velocity saturation of the plant, is a major source of instability in the experimental implementation of SEAs.

Appendix A. Supplementary material

Supplementary data associated with this article can be found, in the online version, at <http://dx.doi.org/10.1016/j.mechatronics.2015.01.007>.

References

- [1] Krebs H, Hogan N, Aisen M, Volpe B. Robot-aided neurorehabilitation. *IEEE Trans Rehab Eng* 1998;6(1):75–87.
- [2] Jezernik S, Colombo G, Morari M. Automatic gait-pattern adaptation algorithms for rehabilitation with a 4-DOF robotic orthosis. *IEEE Trans Rob Autom* 2004;20(3):574–82.
- [3] Gupta A, O'Malley MK, Patoglu V, Burgar C. Design, control and performance of RiceWrist: a force feedback wrist exoskeleton for rehabilitation and training. *Int J Rob Res* 2008;27(2):233–51.
- [4] Kazerooni H, Steger R, Huang L. Hybrid control of the Berkeley Lower Extremity Exoskeleton (BLEEX). *Int J Rob Res* 2006;25(5-6):561–73.
- [5] Guthart GS, Salisbury Jr JK. The intuitive TM telesurgery system: overview and application 2000;1:618–21.
- [6] Marescaux J, Leroy J, Gagner M, Rubino F, Mutter D, Vix M, et al. Transatlantic robot-assisted telesurgery. *Nature* 2001;413(6854):379–80.
- [7] Hogan N. Impedance control: an approach to manipulation. *J Dyn Syst Meas Contr* 1985;107(1):1–24.
- [8] Hogan N, Buerger SP. Interaction control. In: *CRC Handbook on Robotics and Automation*; 2005. p. 1–24.
- [9] Krebs H, Volpe BT, Williams D, Celestino J, Charles SK, Lynch D, et al. Robot-aided neurorehabilitation: a robot for wrist rehabilitation. *IEEE Trans Neural Syst Rehabil Eng* 2007;15(3):327–35.
- [10] Buerger SP, Hogan N. Complementary stability and loop shaping for improved human–robot interaction. *IEEE Trans Rob* 2003;19(2):232–44.
- [11] Siciliano B, Sciavicco L, Villani L, Oriolo G. *Robotics, modelling, planning and control*. Springer; 2009.
- [12] Whitney DE. Force feedback control of manipulator fine motions. *ASME J Dynam Syst Meas Contr* 1977;99(2):91–7.
- [13] Wyeth GF. Control issues for velocity sourced Series Elastic Actuators. In: *Proceedings of the Australasian conference on robotics and automation*.
- [14] Vallery H, Veneman J, van Asseldonk E, Ekkelenkamp R, Buss M, van der Kooij H. Compliant actuation of rehabilitation robots. *IEEE Rob Autom Mag* 2008;15(3):60–9.
- [15] Newman WS, Zhang Y. Stable interaction control and coulumb friction compensation using natural admittance control. *J Rob Syst* 1992;11(1):3–11.
- [16] Colgate JE, Hogan N. Robust control of dynamically interacting systems. *Int J Control* 1988;48(1):65–88.
- [17] Colgate E, Hogan N. An analysis of contact instability in terms of passive physical equivalents 1989:404–409.
- [18] Hannaford B, Ryu J-H. Time-domain passivity control of haptic interfaces. *IEEE Trans Rob Autom* 2002;18(1):1–10.
- [19] Ryu JH, Kwon DS, Hannaford B. Stable teleoperation with time-domain passivity control. *IEEE Trans Rob Autom* 2004;20(2):365–73.
- [20] Tagliamonte NL, Scordia M, Formica D, Campolo D, Guglielmelli E. Effects of impedance reduction of a robot for wrist rehabilitation on human motor strategies in healthy subjects during pointing tasks. *Adv Rob* 2011;25(5):537–62.
- [21] Pratt GA, Williamson MM. Series elastic actuators. In: *Proceedings 1995 IEEE/RSJ international conference on intelligent robots and systems* 95. 'Human Robot Interaction and Cooperative Robots'. IEEE; 1995. p. 399–406.
- [22] Robinson DW. Design and analysis of series elasticity in closed-loop. PhD thesis, MIT; 2000. p. 1–123.
- [23] Robinson DW, Pratt JE, Paluska DJ, Pratt GA. Series elastic actuator development for a biomimetic walking robot. In: *Proceedings 1999 IEEE/ASME international conference on advanced intelligent mechatronics*, 1999. IEEE; 1999. p. 561–8.
- [24] Paluska D, Herr H. The effect of series elasticity on actuator power and work output: implications for robotic and prosthetic joint design. *Rob Auton Syst Special Issue Morphol Control Passive Dyn* 2006;54:667–73.
- [25] Veneman J, Ekkelenkamp R, Kruidhof R, van der Helm F, van der Kooij H. A series elastic- and bowden-cable-based actuation system for use as torque actuator in exoskeleton-type robots. *Int J Rob Res* 2006;25(3):261–81.
- [26] Sulzer JS, Roiz RA, Peshkin MA, Patton JL. A highly backdrivable, lightweight knee actuator for investigating gait in stroke. *IEEE Trans Rob* 2009;25(3):539–48.
- [27] Sensinger JW, Weir RFF. User-modulated impedance control of a prosthetic elbow in unconstrained, perturbed motion. *IEEE Trans Biomed Eng* 2008;55(3):1043–55.
- [28] Sergi F, Chawda V, O'Malley MK. Interaction control of a non-backdriveable MR-compatible actuator through series elasticity. In: *Proceedings of the 6th annual ASME dynamic systems and controls conference*. Palo Alto, CA, October 21–23 2013.
- [29] Gassert R, Chapuis D, Roach N, Wing A, Bleuler H. 2-DOF fMRI-compatible haptic interface for bimanual motor tasks with grip/load force measurement. *Sense Touch Rendering* 2008:109–29.
- [30] Pratt GA, Williamson MM, Dillworth P, Pratt J, Ulland K, Wright A. Stiffness isn't everything. In: *Fourth international symposium on experimental robotics*; 1995. p. 1–6.
- [31] Kong K, Bae J, Tomizuka M. A compact rotary series elastic actuator for human assistive systems. *IEEE/ASME Trans Mechatron* 2012;17(2):288–97.
- [32] Sensinger JW. Improvements to series elastic actuators. In: *Proceedings of the 2nd IEEE/ASME international conference on mechatronic and embedded systems and applications*. IEEE; 2006. p. 1–7.
- [33] Pratt GA, Willisson P, Bolton C, Hofman A. Late motor processing in low-impedance robots: impedance control of series-elastic actuators. *Proc 2004 ACC* 2004:3245–51.
- [34] Vallery H, Ekkelenkamp R, van der Kooij H, Buss M. Passive and accurate torque control of series elastic actuators. In: *IEEE/RSJ International Conference on Intelligent Robots and Systems*; 2007. p. 3534–38.
- [35] Mosadeghzad M, Medrano-Cerda GA, Saglia JA, Tsagarakis NG, Caldwell DG. Comparison of various active impedance control approaches, modeling, implementation, passivity, stability and trade-offs. In: *2012 IEEE/ASME international conference on Advanced Intelligent Mechatronics (AIM)*; 2012. p. 342–48.
- [36] Sergi F, Erwin A, O'Malley MK. Interaction control capabilities of an MR-compatible compliant actuator for wrist sensorimotor protocols during fMRI, in press. In: *IEEE/ASME Transactions on Mechatronics*; 2015.
- [37] Sergi F, Accoto D, Carpino G, Tagliamonte NL, Guglielmelli E. Design and characterization of a compact rotary Series Elastic Actuator for knee assistance during overground walking. In: *2012 4th IEEE RAS & EMBS international conference on biomedical Robotics and Biomechanics (BioRob)*; 2012. p. 1931–36.
- [38] Accoto D, Carpino G, Sergi F, Tagliamonte NL, Zollo L, Guglielmelli E. Design and characterization of a novel high-power series elastic actuator for a lower limb robotic orthosis. *Int J Adv Rob Syst* 2013:1–12.
- [39] Diftler MA, Mehling JS, Abdallah ME, Radford NA, Bridgwater LB, Sanders AM, et al. Robonaut 2-the first humanoid robot in space. In: *2011 IEEE international conference on robotics and automation*. IEEE; 2011. p. 2178–83.